

Evaluation of $y(\text{UTC}(\text{NICT}))$ with respect to NICT-Sr1 for the period MJD 59589 to 59609

We have evaluated the fractional frequency deviation of the time scale $\text{UTC}(\text{NICT})$ for the period from MJD 59589 to 59609 (Jan. 10 – Jan. 30 in 2022) to be $\overline{y(\text{UTC}(\text{NICT}))} = -6.01 \times 10^{-16}$, using secondary frequency standard NICT-Sr1.

NICT-Sr1 measured the mean frequency deviation of hydrogen maser $\text{HM}_{1402014}$ to be $\overline{y(\text{HM}_{1402014})} = -6.9018 \times 10^{-14}$, and the frequency of $\text{UTC}(\text{NICT})$ was then determined by the Japan Standard Time system.

The optical lattice clock acquired data for 47 228 s (2.7% of the total evaluation period) over three operating intervals on MJD 59593, 59600, and 59606 as shown in Fig. 1. The resulting uncertainties are represented in the following table according to Circular T notation:

Period of Estimation (MJD)	$\overline{y(\text{UTC}(\text{NICT}))}$	u_A	u_B	$u_{A/\text{Lab}}$	$u_{B/\text{Lab}}$	u_{Srep}	uptime
59589 – 59609	-6.01	0.32	0.65	1.95	0.22	4	2.7%
Effect	Uncertainty						
$u_{A/\text{Sr}}$	0.32	✓					
u_B	0.65		✓				
HM: linear trend estimation	1.50			✓			
HM: stochastic noise	1.25			✓			
Optical-microwave comparison / microwave transfer	0.22				✓		
Uncertainty of Sr as SRS	4					✓	

Table 1. Results of evaluation. All number are in parts of 10^{-16} .

The evaluation employs the recommended value of the ^{87}Sr clock transition as a secondary representation of the second: $\nu(^{87}\text{Sr}) = 429\,228\,004\,229\,873.0$ Hz with its relative standard uncertainty of $u_{\text{Srep}} = 4 \times 10^{-16}$, determined by the 21st CCTF in June 2017.

u_A is the Type A uncertainty of NICT-Sr1 as an optical standard. It represents the statistical uncertainty determined by interleaved measurements [1].

u_B is the Type B uncertainty of NICT-Sr1 [1 – 3], including the uncertainty of the gravitational redshift.

$u_{A/\text{Lab}}$ and $u_{B/\text{Lab}}$ represent the uncertainty of the link of NICT-Sr1 to $\text{UTC}(\text{NICT})$, consisting of

- Type A uncertainty $u_{A/\text{Lab}} = 1.95 \times 10^{-16}$, which represents the linear trend estimation of the HM ($u_{1/\text{trend}}$) as well as the uncertainty due to the stochastic noise of the HM during unobserved intervals ($u_{1/\text{stoch}}$), and
- Type B uncertainty $u_{B/\text{Lab}} = 2.2 \times 10^{-17}$ due to the frequency comparison between microwave and optical signals, including distribution of the microwave signals.

1. Evaluation of the frequency of hydrogen maser HM₁₄₀₂₀₁₄ with respect to NICT-Sr1 over 20 days

The details of NICT-Sr1 are described in [1, 2]. The Sr atoms were laser-cooled using a two-stage laser cooling technique and loaded to a vertically oriented one-dimensional optical lattice.

We transfer the HM behavior to an Er:fiber comb by stabilizing a heterodyne beat between the 37th harmonic of the frequency comb's approximately 250 MHz repetition rate and a 9.3 GHz signal from a dielectric resonator oscillator (DRO) phase-locked to the 100 MHz signal of HM₁₄₀₂₀₁₄. The optical frequency reference at 698 nm supplied by NICT-Sr1 is measured as a beat with a frequency-doubled output branch of the comb. The comb repetition rate is detected at the output of the same output branch to reduce variations in relative phase, and the system incorporates a temperature-stabilized baseplate to maintain stable optical path lengths. The phase-locked beat signals for carrier-envelope offset and repetition rate are monitored by zero-deadtime counters.

Another frequency comb system operates simultaneously to confirm the measurement results. In this system, the repetition rate is stabilized by phase-lock of the heterodyne beat between the 82nd harmonic of the frequency comb's approximately 100 MHz repetition rate and an 8.2 GHz DRO phase-locked to the 100 MHz signal of HM₁₄₀₂₀₁₄. A transfer laser at 1397 nm is frequency-doubled by a PPLN waveguide. Its output is separated into a visible component used to phase-lock the laser to the optical frequency reference at 698 nm supplied by NICT-Sr1, and a residual infrared component that generates a beat signal with the frequency comb. This beat is counted both directly and through a tracking oscillator to allow rejection of cycle slips.

The counter records and the comparison of the independent combs are used to identify and remove data segments affected by cycle slips or miscounts.

After this confirmation, the fractional deviation of the HM frequency from its nominal value is stored as a pre-averaged value for a series of 10 s bins. Weights are assigned according to the number of contributing data points in each bin.

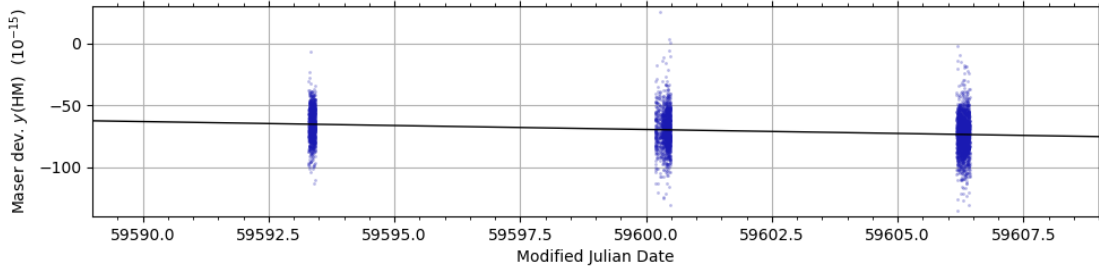


Fig.1. Distribution of maser frequency measurements in terms of fractional deviation $y(\text{HM})$ from the nominal frequency. The black solid line indicates the linear fit used to obtain the mean value over the evaluation interval.

2. Statistical uncertainty of the HM frequency measurement

We determine a statistical uncertainty of the maser frequency measurement $u_{\text{stat}} = 1.46 \times 10^{-16}$ from the residuals of a linear fit by extrapolating the Allan deviation from the region limited by white frequency noise (30–4 000 s) to the full length of available data.

When plotting the instability of the frequency measurements for HM₁₄₀₂₀₁₄ in terms of the Hadamard deviation, we expect a flicker floor $\sigma_L^2 \approx a_{-1}$ due to flicker frequency noise (FFN), and ultimately a growing instability modeled as flicker-walk frequency modulation. These are

described in the following section. Since they are part of the intrinsic HM frequency evolution to be measured, no additional measurement uncertainty is assigned.

There is a difference of $-71\,984$ s between the midpoint (MJD 59599.0) of the evaluation period and the barycenter of the data (approximately MJD 59599.83). The estimation of the maser drift over this time interval introduces an uncertainty of $u_{\text{drift}} = 3.3 \times 10^{-17}$, such that

$$u_{\text{l/trend}} = (u_{\text{stat}}^2 + u_{\text{drift}}^2)^{1/2} = 1.50 \times 10^{-16}.$$

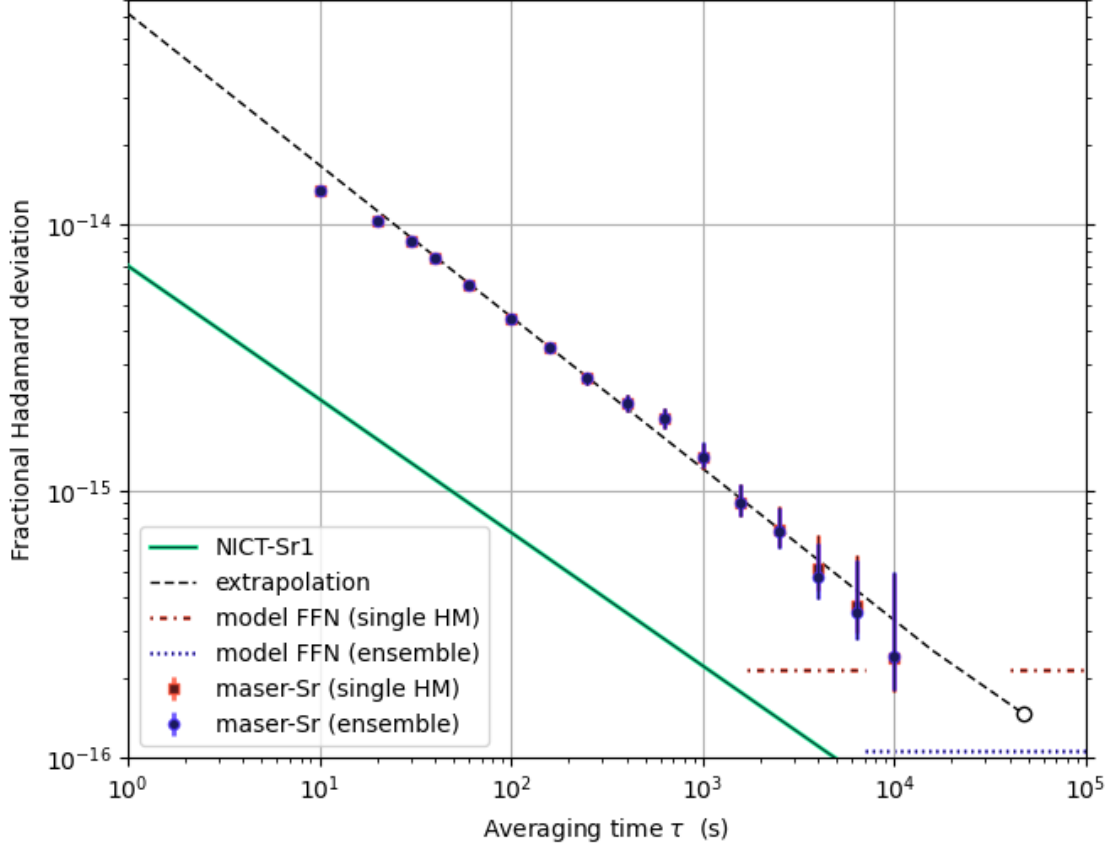


Fig.2. Instability of maser frequency measurements with respect to NICT-Sr1. Blue circles and red squares show the overlapping Hadamard deviation for the residuals from a linear fit with and without correction for deviation of the HM from linear drift, as determined using an ensemble of 4 HMs. Gaps have been removed by contracting the data into a continuous interval. Error bars indicate 1σ uncertainties, calculated for white frequency noise. The black dashed line indicates the extrapolation to the full length of available data, used to obtain the statistical uncertainty indicated by the open mark. For long averaging times, the Hadamard deviation falls to a level consistent with the maser stability model, indicated by the red upper dashed line for a single maser, and by the blue lower dashed line for the ensemble, where the instability is expected to improve by a factor of $1/\sqrt{N_{\text{ens}}}$. The green line shows the instability contribution from NICT-Sr1.

3. Treatment of stochastic noise during unobserved intervals

For intermittent clock operation, phase and frequency excursions of the HM during unobserved intervals contribute significant measurement uncertainty [2, 4].

To mitigate their overall effect, we include a total of four HMs in the evaluation (HM₁₄₀₂₀₀₃, HM₁₄₀₂₀₀₄, HM₁₄₀₂₀₁₂ and HM₁₄₀₂₀₁₄). Their relative phase is continuously monitored by the Japan Standard Time dual-mixer time-difference (DMTD) system [5]. We calculate the frequency difference of each HM from the ensemble average and confirm the absence of abnormal behavior

during the evaluation period. We then determine the frequency of $\text{HM}_{1402014}$ with respect to the ensemble. By subtracting frequency offset and linear trend from this relative frequency, we obtain residuals that approximate the instantaneous deviation of $\text{HM}_{1402014}$ from a pure linear drift, while summing to zero over the evaluation period. We use these residuals (calculated for a set of one-hour intervals) to correct the HM frequency measured with respect to the Sr clock. The result is an improved representation of the mean frequency and linear drift of $\text{HM}_{1402014}$ over the complete evaluation period. A weighted linear fit is applied to the corrected data to find the frequency corresponding to the midpoint of the 20-day interval. The ensemble-based corrections result in a change of the reported HM frequency by 7.9×10^{-17} compared to the result obtained using only $\text{HM}_{1402014}$.

We characterize the typical instability of a single maser based on evaluation of several years of continuous data using three-corner-hat methods, and find that for large averaging times it is well-described by an Hadamard variance $\sigma_{\text{H}}^2(\tau) = a_{-1} + a_{-3} \tau^2$. Here, $a_{-1} = (2.1 \times 10^{-16})^2$ represents flicker frequency noise (FFN) [6] while the slow-varying noise that dominates the long-term instability through $a_{-3} = (1.9 \times 10^{-22}/\text{s})^2$ is typically referred to as flicker-walk frequency modulation (FWFM) [7]. We follow the approach described in the supplement of ref. [8] to determine the uncertainty of extrapolating from arbitrarily distributed data to the full evaluation period. This yields a distribution-specific sensitivity to the HM's noise power spectral density (PSD) [8], which we obtain from the observed maser instabilities a_{-1} and a_{-3} through the relations

$$\text{FFN: } \sigma_{\text{H}}^2(\tau) = \frac{1}{2} \ln\left(\frac{256}{27}\right) h_{-1} \quad \text{for } S_y^{\text{FFN}} = h_{-1} f^{-1} \quad \text{and} \quad (1)$$

$$\text{FWFM: } \sigma_{\text{H}}^2(\tau) = \frac{16}{6} \pi \ln\left(\frac{3}{4} \cdot 3^{11/16}\right) h_{-3} \tau^2 \quad \text{for } S_y^{\text{FWFM}} = h_{-3} f^{-3} \quad , \quad (2)$$

according to refs. [7, 9]. Additional information on the procedure is available in ref. [4]. Despite the complexity of FFN and FWFM in the temporal domain, the noise can always be expressed as a sum over normally distributed sources, and there is no correlation between the noise encountered in separate masers. The maser ensemble therefore shows the same uncertainty reduction with $N_{\text{ens}}^{-1/2}$ as other noise types.

For the present measurement distribution and PSDs, this leads to the uncertainty contributions $u_{1/\text{FFN}} = 1.11 \times 10^{-16}$ and $u_{1/\text{FWFM}} = 5.7 \times 10^{-17}$, which we include as $u_{1/\text{stoch}} = 1.25 \times 10^{-16}$. Since the frequency evaluation for each TAI calibration is performed separately and based on non-overlapping data sets, the uncertainty $u_{1/\text{stoch}}$ represents errors that are uncorrelated between calibrations.

4. Systematic uncertainty for the link of UTC(NICT) to NICT-Sr1

Our intermittent measurements of the maser frequency are easily affected by phase shifts resulting from diurnal temperature variations as well as thermalization effects at the start of operation. Frequency combs and measurement instruments are operated continuously to avoid start-up effects and to maintain a constant heat load in the laboratory. Our evaluation of the systematic lab-side link uncertainty considers the following four sources of systematic errors.

4.1 DMTD measurement of HM–UTC(NICT) over the full reporting interval

Measuring frequencies as phase evolution between near-identical signals over time largely eliminates frequency calibration errors. We search for a residual persistent error by comparing DMTD measurements of the frequency difference $y(\text{HM} - \text{UTC}(\text{NICT}))$ to those of a time interval counter (TIC). Considering all undisturbed operating intervals of six HMs after MJD 59283, the weighted mean of the DMTD – TIC difference is $4.0(5.4) \times 10^{-18}$, limited by the phase noise of the TIC. From this, we set a constraint of $u_{\text{DMTD}}^2 = (4.0 \times 10^{-18})^2 +$

$(5.4 \times 10^{-18})^2 = (6.7 \times 10^{-18})^2$ for the largest expected continuous measurement error of the DMTD measurement of a HM frequency relative to UTC(NICT).

4.2. Diurnal delay variation of distributed HM signals

NICT's HMs are installed in separate environmentally controlled rooms on the third floor of a building adjacent to the one that houses the comb lab on the first floor. The primary measurement reference is a 100 MHz signal that is transferred by coaxial cable and made available to both frequency combs by a distribution amplifier. We investigate the magnitude of delay variations in this system by a looped-back signal transmitted over an additional pair of identically routed cables. An identical distribution amplifier module is also included in this loop. A phase comparator measurement shows slow delay variation within a band of 10 ps width, which results in a negligible frequency error over the full calibration interval.

The predominant uncertainty contribution arises from a daily phase variation, which is similarly sampled by repeated intervals of clock operation. We calculate a Lomb-Scargle periodogram over the nearly continuous phase record since MJD 59486. The elevated energy content in the frequency bin corresponding to 1 cycle/day corresponds to a sinusoidal delay variation with an amplitude of $a_{\text{dist}} = 0.20$ ps. The derivative of the variation yields a maximum fractional frequency error of $\delta y_{\text{max}} = 2\pi a_{\text{dist}}/T$, where $T = 1$ d is the signal period. We take $u_{\text{dist}} = \delta y_{\text{max}} = 1.5 \times 10^{-17}$ as a conservative estimate of the frequency uncertainty. The data does not show any identifiable harmonics with periods of $T = 1$ d/ N .

4.3. Uncertainty of optical-to-microwave comparisons

Both frequency combs similarly determine the clock laser frequency relative to the HM 100 MHz reference. The difference in their results probes delay variations after the distribution amplifier, the radio frequency up-conversion by separate DROs, the comb measurements themselves, and the fiber-noise cancelled distribution of optical signals to the combs. Common HM noise cancels in the difference evaluation, allowing stringent limits to be set.

We determine a difference and instability for each clock operations since MJD 59487. A weighted average yields the difference $\Delta_{\text{comb}} = 7.3(4.0) \times 10^{-18}$. To account for observed overscatter, the individual, statistical variance estimates have been inflated by multiplication with the original reduced $\chi_r^2 = 4.0$. We attribute the observed comb frequency difference to residual cycle slips or miscounts that could not be detected over the HM noise. As these will not equally affect the frequency combs, we take the full difference to set a constraint of $u_{\text{comb}}^2 = (7.3 \times 10^{-18})^2 + (4.0 \times 10^{-18})^2 = (8.3 \times 10^{-18})^2$ for the largest expected persistent measurement error.

4.4 Cyclical variation in measured HM frequency differences

The ensemble correction, applied to reduce the effects of unobserved stochastic HM behavior, introduces a sensitivity to diurnal variations in the HM-to-HM phase differences measured by the DMTD system. We perform a similar analysis as in section 4.2. A periodogram is calculated for the difference of HM₁₄₀₂₀₁₄ and HM₁₄₀₂₀₁₂, which offer the longest available interval of 1054 days. There is no indication of a signal at 1 cycle/day or harmonic multiples. The long averaging interval maximizes the resolution, but the HM noise energy content in this frequency bin only allows the sinusoidal delay variation to be constrained to an amplitude of $a_{\Delta\text{HM}} = 0.17$ ps, for which we assign an uncertainty of $u_{\Delta\text{HM}} = 1.2 \times 10^{-17}$ as before. For simplicity, we currently neglect any reduction in expected error from averaging over multiple different channels of the DMTD, and from the contribution of the original maser (with a weight of $1/N$ for N HMs), which does not require a difference measurement.

4.5 Overall uncertainty

We combine the systematic uncertainties to find $u_{\text{B/Lab}}^2 = u_{\text{DMTD}}^2 + u_{\text{dist}}^2 + u_{\text{comb}}^2 + u_{\Delta\text{HM}}^2 = 2.2 \times 10^{-17}$ based on the currently available data. A manuscript is in preparation to provide a more detailed description of the reassessment of the systematic lab-side link uncertainty.

5. Frequency deviation of UTC(NICT)

The frequency difference between $\text{HM}_{1402014}$ and UTC(NICT) over the evaluation period is calculated as

$$y(\text{UTC(NICT)} - \text{HM}_{1402014}) = (\delta_a - \delta_b)/T, \quad (3)$$

where δ_a and δ_b represent the time difference $\text{UTC(NICT)} - \text{HM}_{1402014}$ at the beginning and end of an evaluation interval of length T . These values are continuously measured by the DMTD system [5] and reported to BIPM, where they are used in the EAL generation and made available at <https://webtai.bipm.org/ftp/pub/tai/data/>. A comparison to the independent TIC data is used to inspect the data for measurement errors.

6. Accuracy of NICT-Sr1

The systematic corrections and their uncertainties for NICT-Sr1 [1 – 3] are summarized below:

Effect	Correction (10^{-17})	Uncertainty (10^{-17})
Blackbody radiation	506.8	1.5
Lattice scalar / tensor	0	5.3
Lattice hyperpolarizability	-0.2	0.1
Lattice E2/M1	0	0.5
Probe light	0.1	0.1
Dc Stark	0.1	0.2
Quadratic Zeeman	51.5	0.3
Density	0.6	0.4
Background gas collisions	0	1.8
Line pulling	0	0.1
Servo error	-0.6	1.9
Total	558.2	6.2
Gravitational redshift	-834.1	2.2
Total (with gravitational effect)	-275.9	6.5

Table 2. Systematic corrections and their uncertainties for NICT-Sr1.

7. References

- [1] H. Hachisu and T. Ido, “Intermittent optical frequency measurements to reduce the dead time uncertainty of frequency link,” *Jpn. J. Appl. Phys.* **54**, 112401 (2015).
- [2] H. Hachisu, G. Petit, F. Nakagawa, Y. Hanado and T. Ido, “SI-traceable measurement of an optical frequency at low 10^{-16} level without a local primary standard,” *Opt. Express* **25**, 8511 (2017).
- [3] H. Hachisu, F. Nakagawa, Y. Hanado and T. Ido, “Months-long real-time generation of a time scale based on an optical clock,” *Sci. Reports* **8**, 4243 (2018).
- [4] N. Nemitz *et al.*, “Absolute frequency of 87Sr at 1.8×10^{-16} uncertainty by reference to remote primary frequency standards,” *Metrologia* **58**, 025006 (2021)
- [5] F. Nakagawa *et al.*, “Development of multichannel dual-mixer time difference system to generate UTC(NICT),” *IEEE Trans. Instrum. Meas.* **54**, 829 (2005).
- [6] D. Allan, “Time and frequency (time-domain) characterization, estimation, and prediction of precision clock and oscillators,” *IEEE UFFC* **34**, 647 (1987).
- [7] W. J. Riley, “Handbook of Frequency Stability Analysis,” NIST Special Publication 1065 (2008)
- [8] C. Grebing *et al.*, “Realization of a timescale with an accurate optical lattice clock,” *Optica* **3**, 563-569 (2016).
- [9] S. T. Dawkins, J. J. McFerran and A. Luiten, “Considerations on the Measurement of the Stability of Oscillators with Frequency Counters,” *IEEE Trans. UFFC* **54**, 918-925 (2007).